COAGULATION MODELING OF AN ARTERY: A COUPLED CHEMICAL-MECHANICAL APPROACH

An Undergraduate Research Scholars Thesis

by

DOMINIC ISAIAH JARECKI

Submitted to the Undergraduate Research Scholars program at
Texas A&M University
in partial fulfillment of the requirements for the designation as an

UNDERGRADUATE RESEARCH SCHOLAR

Approved by Research Advisor: Dr. Arun Srinivasa

May 2017

Major: Mechanical Engineering

TABLE OF CONTENTS

ABSTRACT

Coagulation Modeling Of an Artery: A Coupled Chemical-Mechanical Approach

Dominic I. Jarecki
Department of Mechanical Engineering
Texas A&M University

Research Advisor: Dr. Arun Srinivasa
Department of Mechanical Engineering
Texas A&M University

Literature Review

Heart disease is a leading cause of death in developed countries. It typically is a slow killer, with atherosclerosis slowly worsening throughout the course of a patient's lifetime, often only revealing itself with traumatic circulatory failure such as heart attack or stroke. To combat heart disease in the long term, then, requires not just knowledge of a traumatic event itself, but also the slow progression that leads up to it. To this end, extensive research of the circulatory system has been performed to study blood flow fields formed and their interplay with coagulation phenomena.

The flow behavior of blood is influenced by many factors. Most notably, the mechanical behavior of the blood flow and the blood vessel walls, the chemical composition of the blood, and the presence of geometric irregularities—whether due to genetic defects, injuries, or the addition of man-made objects (for instance stents or LVADs) to treat a particular health issue—make complete analysis difficult. The associated computational cost makes full-scale preventative simulation (perhaps carried out over a lifetime) prohibitive.

Focusing on mechanics based simulations, work with varying degrees of fidelity has been performed, usually with the data of interest including the local blood pressure, wall shear stress, and flow patterns ([1], [2]), and usually limited to studies of arteries.

Early simulations often assumed the arterial wall to be rigid, the blood to be a Newtonian fluid, or both (see [3], [4]), a choice necessitated by the computational challenges of coupled fluid-structure interaction (FSI) and variable viscosity behavior.

Simulations with varying levels of sophistication including details such as patient specific data, three-dimensional models, and fluid-structure interaction (FSI) between the blood and arterial walls ([5], [6], [7]) have been performed, albeit usually limited to a particular blood vessels (such as the carotid or iliac artery bifurcations) exclusively.

Analyses in these works have been predominantly focused on the mechanical behavior of an system whose response does not evolve; that is, stress-strain phenomena in the walls and velocity and stress of the blood flow are investigated in some system with a given (constant) degree of stenosis. In reality, the vascular system is the stage for constant chemical activity, which can alter not only the geometry (for instance increasing clotting in an area and restricting flow) but also mechanical properties such as the local viscosity of the blood and the rigidity of the arterial walls themselves.

Research into the chemical behavior of the coagulation cascade has largely proceeded separately from the analysis of the mechanical phenomena observed; this is in part due to the complexity of the models that govern this behavior ([8], [9]).

This difficulty is shown particularly in regards to modeling of platelet action. Coagulation in the vascular system is effected by synergistic mechanical action of platelets and chemical reaction of the clotting factors that make up the coagulation cascade. Due to the immense number of platelets present in blood (roughly 200 000 platelets/μL of blood for a healthy human adult) they present significant tracking difficulty, and most modeling efforts are limited to blood vessels on the order of capillaries or arterioles to keep the number of platelets

manageable (see [10]–[12]). However, most of the important clotting pathologies manifest themselves in larger blood vessels, such as the carotid.

Predictive and diagnostic modeling patient-specific simulation requires that an appropriate balance be struck between accuracy and accessibility and between scope and detail. Previous work by the authors of this study investigated the consequences of neglecting a non-Newtonian viscosity model, observing how Newtonian and non-Newtonian assumptions affected the stagnation zone size predicted downstream of a mildly stenosed area in an axisymmetric model of an artery.

The goal of this work is to move towards accounting for the chemorheology of flowing blood, with enough simplification to enable rapid evaluation of the response. This paper assesses the feasibility of a reduced-order model of the coagulation cascade coupled with a stochastic model of platelet motion and species convection, laying groundwork for more detailed simulation and clinical implementation designed to remain computationally tractable for use in large arteries.

Thesis Statement

This research work mathematically characterizes a model of coagulation dynamics, coupling a mechanical flow simulation with a reduced-order model of the coagulation cascade and a stochastic advection/diffusion equation to handle platelet motion and species convection. The coupled model is demonstrated in a two-dimensional reduction of an artery.

Theoretical Framework

This work relies on the basic principles of fluid mechanics of a continuum; in addition to these, variable viscosity and other unique properties of blood must be addressed through additional equations.

Project Description

This project introduces a simplified framework for modeling coagulation behavior in the vascular system, and demonstrates the response obtained in quiescent flow. Full implementation requires simulation of blood flow models, stochastic convection of active species, use of a set of reduced-order coagulation chemistry equation, and combination of the three models, potentially in a multi-scale set up.

ACKNOWLEDGEMENTS

I would like to thank my research advisor, Dr. Arun Srinivasa, for his guidance and support throughout this research; his enthusiasm and love of learning always inspire me. I would also like to thank members of our research group, in particular Naveen Thomas and Jayavel Arumugam for their help and critique.

Thanks also go to my other friends and colleagues and the department faculty and staff for making my time at Texas A&M University a great experience. Finally, thanks to my parents and siblings for their encouragement.

INTRODUCTION

The formation (or lack thereof) of clots in the vascular system lies at the center of the vast majority of cardiovascular pathology; for this reason, significant effort in understanding their formation and regulation is warranted. Computational study offers unique opportunity to perform detailed, non-invasive research of these phenomena.

Clots are produced in the vascular system due to the synergistic mechanical action of platelets and chemical reaction and activation of enzymes in the coagulation cascade.

In the extrinsic pathway (which is injury activated and the most physiologically relevant) a wound in the vascular wall exposes tissue factor (TF) and collagen. Tissue factor bonds to free-floating factor VIIa (the formation from VII encouraged by the presence of the injury) producing the active enzyme TF-VIIa. This in turn cleaves the peptide bond of X, forming Xa, and finally, Xa, when associated with factor Va as prothrombinase, catalyzes the production of thrombin (IIa) from prothrombin (II).

Thrombin holds a central role in the process, converting fibrinogen (I) into the insoluble fibrin (Ia), which precipitates out of the blood and forms a mesh over the injury site. Action by factor XIII causes the mesh to crosslink, strengthening it. When the clot is no longer needed, the fibrin mesh is dissolved under the action of plasmin.

This chemical behavior describes only half of the picture, however. Most clots formed *in vivo* consist of less than 1% fibrin by volume (see [13]); the vast majority of a clot's volume is contributed by cellular material (predominantly platelets).

Platelets, small discoid blood cells, float through the blood stream largely inert until activated by the presence of certain chemicals (including ADP, collagen, and thrombin), high shear, or long periods in regions of stagnant flow.

Once activated, platelets undergo morphological change (extending pseudopods outward), release chemicals to encourage activation of other platelets, and begin to aggregate together.

This growing platelet aggregate, attracted to the injury in the wall by the localized release of clot-encouraging chemical species (including ADP, exposed collagen, and thrombin), adheres and constitutes the bulk of the clot. The fibrin mesh plays a critical role in maintaining clot form and retaining platelets under the shear of blood flow through the vessel.

It is evident from the foregoing discussion that both chemical and platelet behavior play a critical role in the formation of a clot and neither is sufficient without the other. Simulating both phenomena presents unique challenges, however; in particular, the sheer number of reacting species and platelets, make straightforward implementation of a computational model impractical for clinical use. In this work, multiple simplifications of the coagulation process are analyzed with the intent of reducing the necessary computational load required to obtain clinically useful results.

CHAPTER I

ALGORITHM OVERVIEW

In this study, the processes of coagulation described in the introduction are simplified and resolved numerically in multiple scales.

To perform the modeling of clot formation and viscosity change in the 2D representation of an artery segment used in this study, the following two algorithms are proposed; one used for the quiescent (no advection) model demonstrated in this work, and the other for the expansion to general flow scenarios. (Both models expand naturally to three dimensions, but are described in two for simplicity of presentation.)

The relevant section of this paper is highlighted for each algorithm; this outline should be kept in mind as the various pieces of the model are studied.

Quiescent Coagulation Study

1. **(Chemical Convection)** The chemical species are allowed to freely diffuse for a single time step (Chapter IV).
    a. Reaction begins in cells immediately adjacent the injury zone
    b. If thrombin concentration in any cell is greater than zero, k_A is set to a reacting value in that cell, adding that cell to the reaction zone
2. **(Chemical Reaction)** Chemical reaction products are computed using current species concentrations at every spatial point in the reaction zone (a subset of the entire geometry determined by a minimum concentration of thrombin in the area). (Chapter III)

Integrated Flow Field Model

3. **(Flow Field)** Using CFD code and the macroscopic geometry, the flow field is determined, using local viscosities existing at the beginning of the time-step, iterating until convergence is reached for this single time step (see Chapter II).
4. **(Chemical Convection)** Using the determined u- and v-velocities of the flow field, the chemical species are convected for a single time step (Chapter IV).
    a. Reaction begins in cells immediately adjacent the injury zone
    b. If thrombin concentration in any cell is greater than zero, k_A is set to a reacting value in that cell, adding that cell to the reaction zone
5. **(Chemical Reaction)** Chemical reaction products are computed using current species concentrations at every spatial point in the reaction zone (a subset of the entire geometry determined by a minimum concentration of thrombin in the area). (Chapter III)
6. **(Platelet Transport and Activation)** Platelet motion is determined using the probabilistic model outlined in this paper (Chapter IV).
    a. If thrombin concentration reaches a threshold value in a cell, platelets in that cell are considered activated and not allowed to leave
    b. If platelet number in a cell reaches a threshold value, no additional platelets are allowed to enter
7. **(Flow Simulation Update)** If any quantities such as local viscosity, chemical concentrations, and platelet aggregate formation are changed by the reacting processes, then they are updated in the macroscopic geometry and the simulation recalculates the flow field. Otherwise, the same flow field is recycled.

Platelet and chemical behavior is considered statistically. Many details of the physiological mechanisms are simplified or ignored in this study, with the goal of demonstrating a much less

computationally demanding framework—which can easily be scaled up to include additional species and greater complexity if necessary—for analyzing coagulation in the vascular system.

CHAPTER II

MECHANICAL MODEL BACKGROUND

Before evolution of a forming clot near an injury *in vivo* can be considered, the overall flow field must be determined. Though not implemented here (for reasons discussed in the following sections), a framework suitable for determination of the flow field—building on previous work by the authors which focused exclusively on the flow field—with suggested models and potential approximations are described below.

Finite-volume discretization of the Reynolds transport equation (such as that employed by the commercial software Star-CCM+ [14]) allow for numerical solution of the flow fields. The most general expressions employed for continuity and momentum (referenced in the user guide) are given below as:

$$\frac{\partial}{\partial t}\left(\int_V \rho\right) dV + \oint_A \rho \mathbf{v} \cdot d\mathbf{a} = \int_V S_u dV \tag{1}$$

$$\frac{\partial}{\partial t}\left(\int_V \rho\, \mathbf{v}\right) dV + \oint_A \rho \mathbf{v} \otimes \mathbf{v} \cdot d\mathbf{a} = -\oint_A p\mathbf{I} \cdot d\mathbf{a} + \oint_A \mathbf{T} \cdot d\mathbf{a} + \int_V \mathbf{f_b}\, dV \tag{2}$$

Where ρ is the density of the fluid, $\mathbf{v}$ is the velocity vector in a stationary reference frame, $\mathbf{a}$ is the area vector, p is the pressure, V is the volume, $\mathbf{I}$ is the identity matrix, $\mathbf{T}$ is the stress tensor, and $\mathbf{f_b}$ is the body force exerted over the volume considered in the simulation.

The shear-thinning behavior of blood can be treated with the Carreau-Yasuda model (as in [3]) under which the viscosity varies as:

$$\frac{\eta - \eta_\infty}{\eta_0 - \eta_\infty} = [1 + (\lambda\dot{\gamma})^a]^{\frac{n-1}{a}} \tag{3}$$

Where η is the dynamic viscosity, n is a power constant—roughly indicating the degree of shear-thinning behavior present—, $\dot{\gamma}$ is the shear rate, η_0 and η_∞ are the viscosities approached as shear rate approaches zero and increases without bound, respectively, and λ and a are fit constants. (If $a = 2$, the model reduces to the Carreau model.)

The material data and boundary conditions used were from several different sources. The viscosity data was taken from Gijsen et al. 1998 [3], but the value for density was changed to be more consistent with that of whole blood ($\rho = 1060\ kg/m^3$ instead of $\rho = 1410\ kg/m^3$). The material parameters are as follows: $\eta_0 = 22(10^{-3})Pa * s$, $\eta_\infty = 2.2(10^{-3})Pa * s$, $a = 0.644$, $n = 0.392$, $\lambda = 0.110\ s$.

The boundary conditions (inlet speed and outlet pressure) used by the author of this study in previous work were based on a simplification of pulsatile waveforms (recorded for healthy adult patients) found in Zhao et al. 2002 [15]. Velocity was obtained in their study using Doppler anemometry near the carotid artery of a living subject (fully developed profiles at the inlet are assumed there and here); pressure was determined in a nearby region using an external pressure transducer.

The following simplified equations were used:

$$\dot{V} = \begin{cases} 4\ \text{mL/s} & 0 < t < 0.2\ \text{s} \\ \left(9 \sin\left((t - 0.2)\left(\frac{10\pi}{3}\right)\right) + 4\right)\ \text{mL/s} & 0.2 \leq t < 0.5\ \text{s} \\ 4\ \text{mL/s} & 0.5 \leq t < 1\ \text{s} \end{cases} \tag{4}$$

$$\bar{v} = \frac{\dot{V}}{\pi R^2} \qquad \left(\frac{\mathrm{m}}{\mathrm{s}}\right) \tag{5}$$

Where $\dot{V}$ is the volumetric flow rate (mL/s), t is time, and R is the radius of the tube in millimeters.

For Newtonian fluid flow through a pipe, the exact solution for fully developed flow shows that the velocity distribution is quadratic across the pipe cross-section. For non-Newtonian behavior, the resulting distribution will be flatter in the center (with higher velocity gradients at the wall) than in the Newtonian case, and so a fourth-order polynomial was used as a quick approximation:

$$v_{NN}(r^*) = \left(\frac{5\bar{v}}{4}\right)(1 - (r^*)^4) \qquad (\mathrm{m/s}) \tag{6}$$

Where $r^* = r/R$ is the normalized radius. The pressure crest at the outlet tends to lag the velocity crest, so the pressure waveform was defined as:

$$P = \begin{cases} 10^3 \text{ Pa} & 0 \leq t < 0.3 \text{ s} \\ 6000 \sin^2\left((t - 0.3)\left(\frac{10\pi}{3}\right)\right) + 10^3 \text{ Pa} & 0.3 \leq t < 0.6 \text{ s} \\ 10^3 \text{ Pa} & 0.6 \leq t < 1 \text{ s} \end{cases} \tag{7}$$

Where $\sin^2(t)$ was chosen, as opposed to $\sin(t)$, to differentiate the width of the waveforms somewhat, qualitatively moving closer to the observed values shown graphically in Zhao et al. 2002 [15]. The heart rate used in this study was 60 BPM, which, conveniently, gives a complete pulse in 1 second. Pressure and volumetric flow rate are shown in Figure 1.

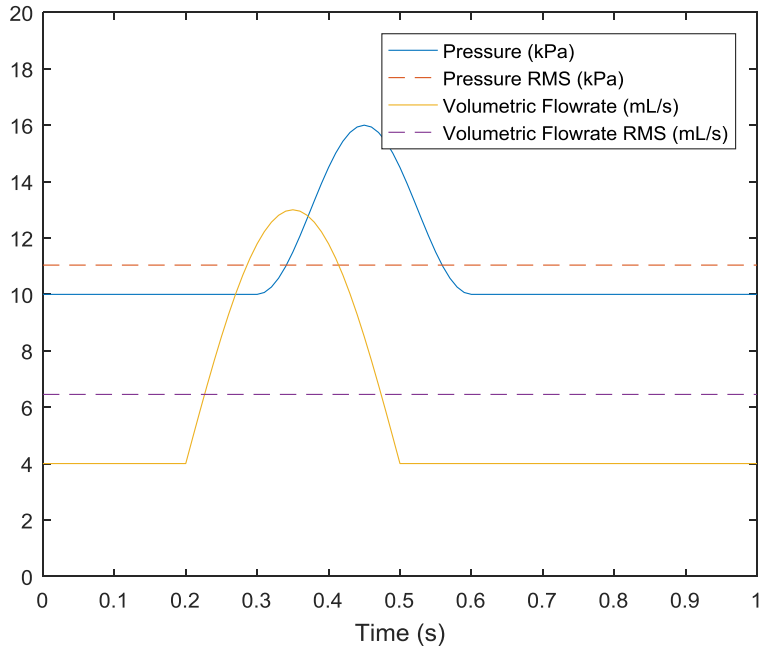

Figure 1. Volumetric flow rate specified at the inlet and backpressure specified at the outlet for a single heart beat in previous study

Due to the prolonged time scale at which clotting occurs (≈20 min or 1200 s), it is likely not important to use a pulsatile waveform for each second in a preliminary study. In this case, the stochastic transition model and reduced-order chemical ODEs are to be tested, but without advanced fluid-structure interaction and modeling of the high shear breakoff behavior of the platelet mass that forms, pulsatile flow behavior is not likely to dramatically influence the final outcome.

As such, root mean square values for the volumetric inlet flow rate and pressure outlet are used here:

$$\dot{V}_{inlet,RMS} = 6.4523 \text{ mL/s} \tag{8}$$

$$\bar{v} = 0.3286 \text{ m/s} \tag{9}$$

$$P_{outlet,RMS} = 11.0377 \text{ kPa} \tag{10}$$

Where $\dot{V}_{inlet,RMS}$ is used with equations (5) and (6).

In a previous research work by the author, three 2.5 mm radius, 75 mm length, axisymmetric representations of arteries (with varying degrees of stenosis—60, 75, and 80% by area) were used. In this work, a two-dimensional slice of these geometries—with no initial stenosis—is used. This keeps the resulting flow fields similar, but allows for observation of clot growth near an injury in the arterial wall.

A rectilinear grid was used in the quiescent study, chosen to be appropriate for use with the flow study so direct comparison can be made. Finer mesh is present in the area near the "injured" section (in which the coagulation reaction is initiated in either case), as shown below (see Figure 2).

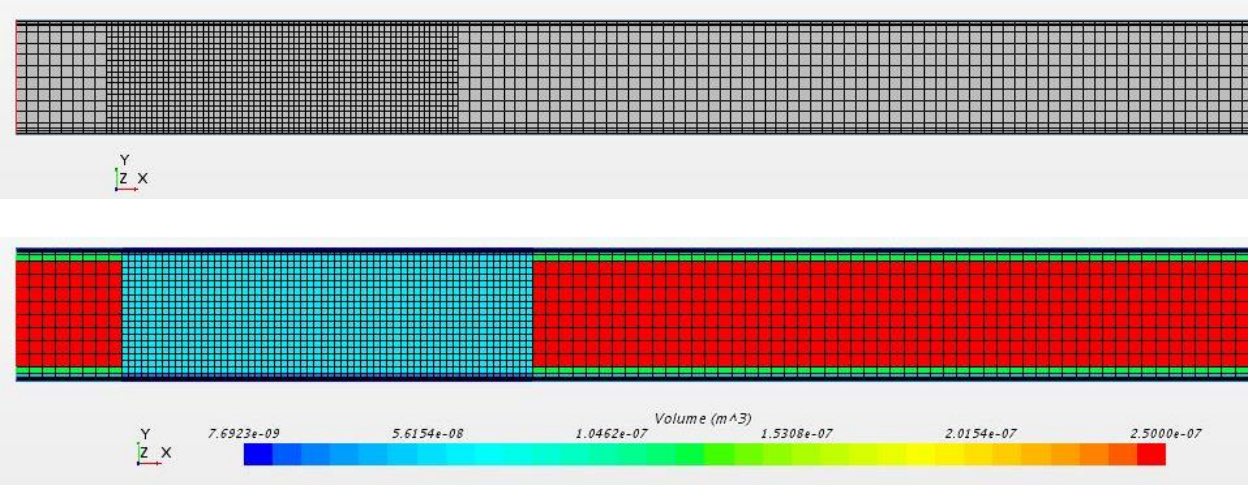

Figure 2. (a) 2D mesh used over the computational domain; (b) Values for cell volume

CHAPTER III

COAGULATION CHEMISTRY MODEL

Background and Rationale

The coagulation cascade involves a complex, highly regulated set of reactions intended to produce clots and maintain vascular integrity against injury (see Figure 3).

Excellent models describing the kinetic behavior during reaction of the more than thirty species involved have been developed (see [9]). However, the time required to obtain a numerical solution at a single point renders computation over an entire spatial domain (in tandem with a flow simulation) intractable.

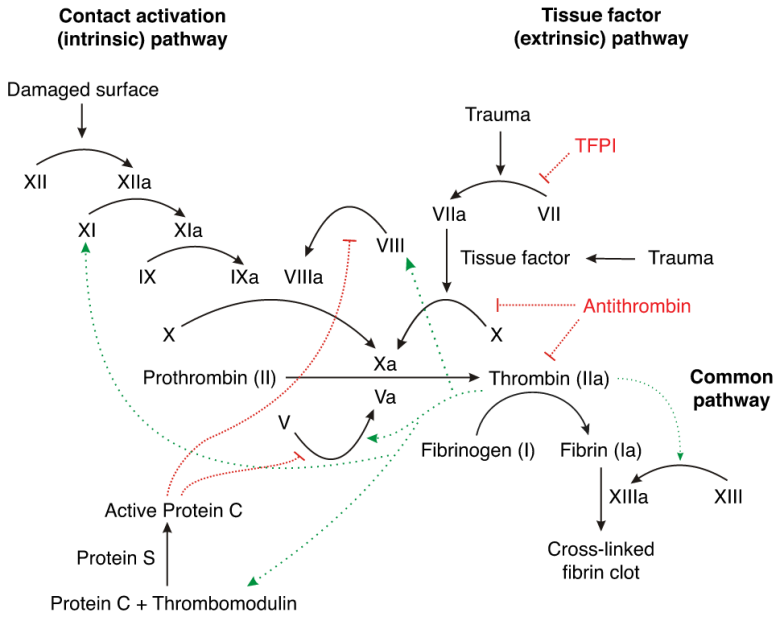

Figure 3. The chemicals involved in the formation and regulation of Thrombin (IIa), the biochemical ultimately responsible for catalyzing the formation of Fibrin (Ia) and the construction of a clot (image source: [16])

As seen in this figure, the aim of both extrinsic and intrinsic clotting pathways is the production of thrombin (factor IIa). Thrombin catalyzes soluble fibrinogen into insoluble fibrin, which, when acted upon by factor XIIIa, creates a cross-linked mesh, key to maintaining stability of the clot, though not sufficient (see Chapter IV) in itself to constitute a clot.

A reduced order model proposed by one of the researchers in our lab ([17]) attempts to describe the most salient features of the coagulation cascade by focusing on the production of thrombin. With an appropriate fit, (in this case to the model used in Danforth et al. [9]) this reduction can be used to quickly replicate the concentrations predicted by a full model with only prothrombin (factor II), thrombin (IIa), antithrombin (AT), and IIa-ATIII.

The four governing differential equations that constitute the reduction of the coagulation model are as follows:

$$\frac{dC_{II}}{dt} = -k_S C_{II} - k_A C_{II} C_{IIa} \tag{11}$$

$$\frac{dC_{IIa}}{dt} = k_S C_{II} + k_A C_{II} C_{IIa} - k_I C_{IIa} C_{AT} \tag{12}$$

$$\frac{dC_{AT}}{dt} = -k_I C_{IIa} C_{AT} \tag{13}$$

$$\frac{dC_{IIa-ATIII}}{dt} = k_I C_{IIa} C_{AT} \tag{14}$$

Essentially, these equations determine thrombin concentration by considering its production from prothrombin and regulation by antithrombin (which produces the inactive reaction product IIa-ATIII).

Reduced-Order Model Assessment

A programmatic method of fitting the coefficients in the reduced-order model was devised, and this was used to determine suitable values for the coefficients k_S, k_A, and k_I that replicate performance by the full model.

Results for a single run are shown below in Figure 4.

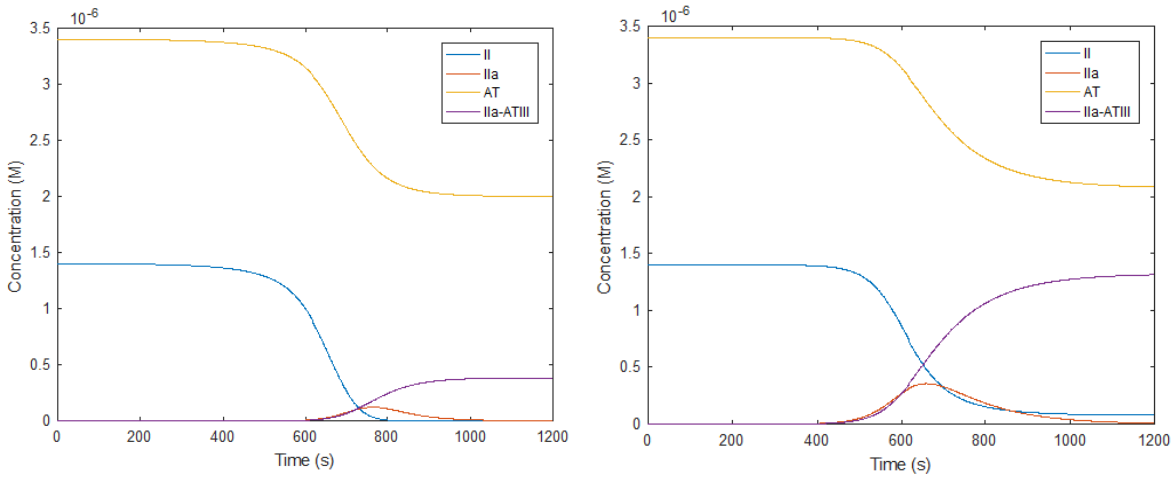

Figure 4. (a) Full model of coagulation cascade results, (b) reduced model results with fit parameters

To assess the robustness of the model, the same process was employed for hundreds of test points, varying the initial concentrations of clotting factors over physiological ranges provided in Table 1.

Following a Latin Hypercube test design, values were chosen, constants k_S, k_A, and k_I were found, and normalized error (difference between full model and the approximate reduced-order model species concentrations) was computed as:

$$\varepsilon_{norm} = \sum_{i=1}^{4} \frac{\left\| C_i^{full} - C_i^{reduced} \right\|_2}{C_i^0} \tag{15}$$

Where C_i^{full} is the vector of concentrations for the *i*th reacting species predicted by the full model and $C_i^{reduced}$ that predicted by the reduced-order fit, for the entire simulation time, $C_i^0$is the initial concentration of the *i*th reacting species, $\|\cdot\|_2$ is the L2 norm, and the summation is carried out over the four species included in the reduced order model.

Table 1. Initial concentration and average ranges of coagulation bio-chemicals for apparently healthy population (see [9])

	Initial Concentration (M)	**Normal Range (%)**
VII	1.00E-08	60 - 140
VIIa	1.00E-10	60 - 140
X	1.60E-07	60 - 140
IX	9.00E-08	69 - 151
II	1.40E-06	60 - 140
VIII	7.00E-10	64 - 232
V	2.00E-08	60 - 140
TFPI	2.50E-09	46 - 171
AT	3.40E-06	88 - 174

Configuring the optimization code to run in parallel, results were obtained in reasonable time using the supercomputer Ada. Some of these are shown in the figures below.

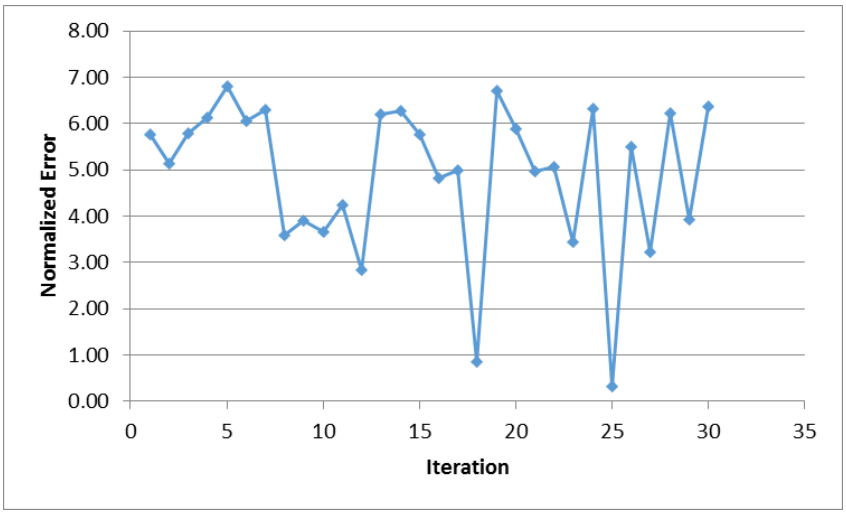

Figure 5. Normalized error over 30 points chosen using the Latin Hypercube experiment design

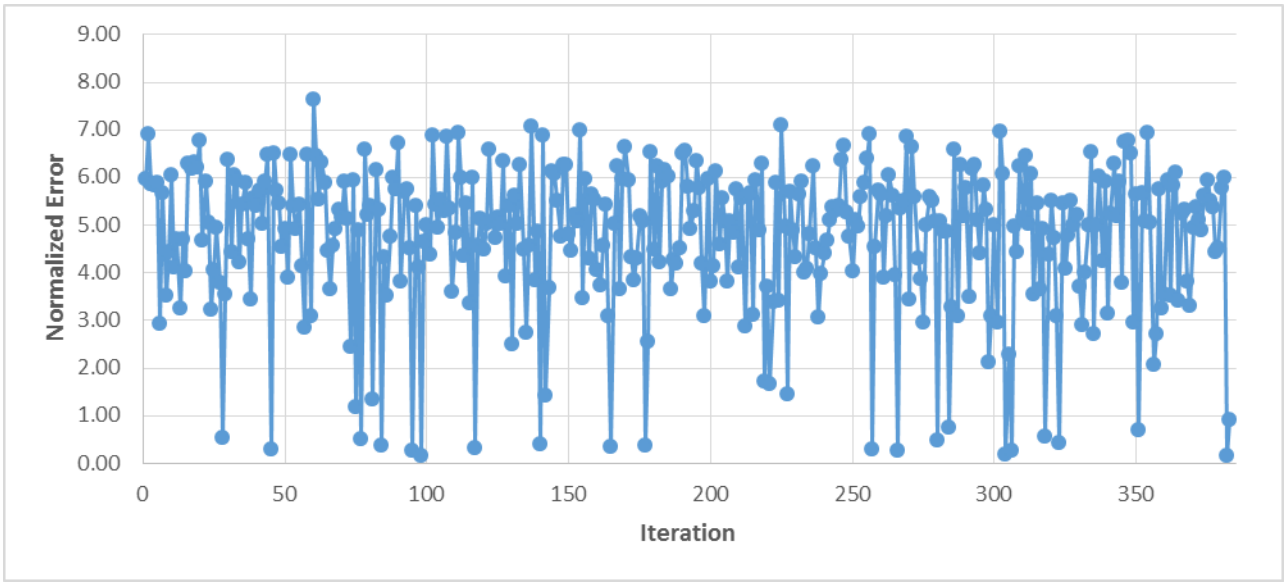

Figure 6. Normalized error over 382 points chosen using the Latin Hypercube experiment design

The normed error was acceptably low (<9; for comparison, in Figure 4, the normed error is about 7) for all the data points; this indicates that the model is acceptably reliable for use in mechanical simulation.

Reduced-Order Model Fit

The values of k_S, k_A, and k_I obtained above were determined for in each case for a *single* set of initial concentrations. However, in a mechanical flow simulation, chemical concentrations (and thus, the initial concentrations for the reactions carried out each time step) vary over the domain.

To be useful for pairing with a mechanical simulation, the normalized error associated with the predicted concentrations cannot become too great for values encountered in the domain.

Danforth et al. [9] indicates that the full model is initiated by introducing 5 pM concentration of TF to the system. In the reduced-order model, prothrombin behavior controls the production of thrombin.

To determine suitable ranges for k_S, k_A, and k_I, average physiological values were taken (Table 1) for the initial concentrations of species in the bloodstream before injury. TF was varied over the range (0, 5) pM, and the resulting values fork_S, k_A, and k_I were observed (see Figure 7).

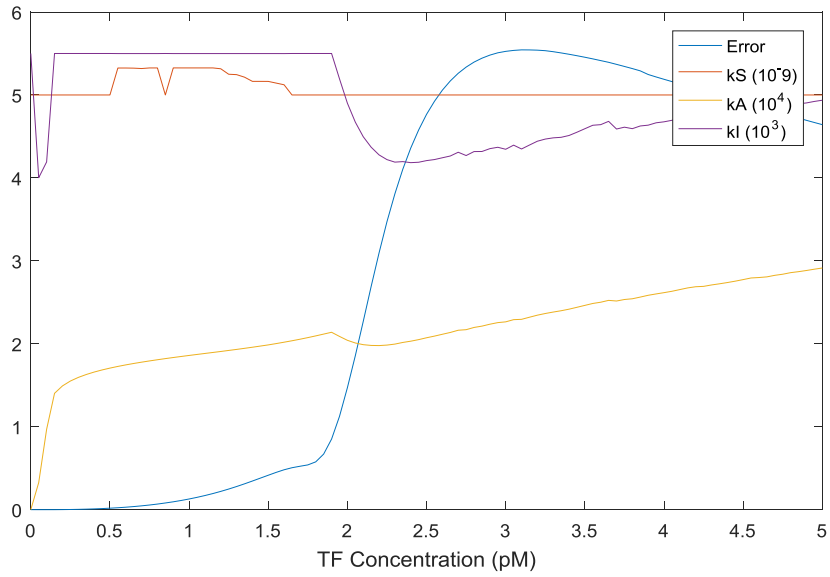

Figure 7. Variation of reduced-order coefficients and normalized error with varying initial TF

Only k_A exhibits a distinct trend, with higher values for larger initial concentrations of TF and, notably, a value of zero for the steady-state case in which no TF is present and no reaction occurs.

The other two coefficients erratic behavior is likely due to the imperfection of the optimization method used to minimize the error between the reduced and full models; it only uses a finite number of points on a finite interval of possibilities for the three coefficients, so some imprecision is to be expected.

It makes sense that k_A exhibits TF-dependent behavior; it functions as a sort of "gas pedal" for the key clotting reaction in which prothrombin is converted into thrombin. To avoid the additional computational burden of convecting and reacting the actual species that trigger the extrinsic pathway (TF with VII to VIIa, producing TF-VIIa or "tenase"; X to Xa acted on by tenase; and finally, the formation of Xa-Va, or "prothrombinase", which will allow the production of thrombin (IIa) from prothrombin (II)), the value of the constants in a cell is used to determine whether species react. The reaction starts in injured cells that have constant values corresponding to a 0.5 pM TF trigger; as thrombin concentration becomes non-zero in the surrounding cells, their k_A values are flipped, and the reaction is allowed to spread.

Table 2. Values of reduced-order model constants used in this study

	Inactive	**Reacting**
$\boldsymbol{k_S}$	$5.0(10^{-9})$	$5.0(10^{-9})$
$\boldsymbol{k_I}$	$4.9363(10^{3})$	$4.9363(10^{3})$
$\boldsymbol{k_A}$	0	$2.9138(10^{4})$

CHAPTER IV

STOCHASTIC SPECIES TRANSPORT

Theory and Rationale

A typical finite volume implementation of the diffusion/advection equation to accomplish transport of species can tie up significant computational resources, especially as the number of species increases. Using a stochastic model could provide a reasonably accurate simplification.

Given *M* cells, consider the probability $P(J|I,t)$ that some of the $N(I,t)$ particles in cell *I* move to cell *J* at the end of time step Δt. If migration between each of the *M* cells is considered, it is evident that:

$$N(J,t+\Delta t) = \sum_{I=1}^{M} P(J|I,t)N(I,t) \tag{16}$$

That is, the number of particles in cell *J* at time $t+\Delta t$ is equal to the number of particles that enter *J* from all cells (including itself). We obtain a transition matrix when considering this process for all cells.

An appropriate expression for the probability function $P(J|I,t)$ can be found by considering continuous solutions to the convection equation.

Spread of a chemical species throughout a medium is given by the differential equation:

$$\frac{\partial c}{\partial t} = -\nabla \cdot \vec{q} \tag{17}$$

Where c is the concentration of the chemical, and $\vec{q}$ is the flux. Under advection, the flux is given as:

$$\vec{q} = c\vec{v} - D\nabla c \tag{18}$$

And

$$\frac{\partial c}{\partial t} = -\vec{v} \cdot \nabla c + D\nabla^2 c \tag{19}$$

Where $\vec{v}$ is the medium flow velocity and D is the diffusion constant. For a dirac delta type release in an infinite plane, with initially zero concentration, it can be shown that the solution to this equation is:

$$c(t) = \left(\frac{1}{2\pi Dt}\right)^n e^{-\frac{(\vec{r}-\vec{v}t)^2}{2Dt}} \tag{20}$$

Where r is a radial coordinate, t is time, and n is an exponent that depends on the dimensionality.

For zero velocity, concentration decays around a central peak as a bell curve; with the addition of advection (and non-zero velocity), the center and shape of the bell curve are skewed somewhat.

Because equation (19) is linear, solutions due to multiple point releases over a domain can be combined as a linear combination. Discretizing equation (20) over a spatial domain with time steps Δt, the denominator normalizing factor for the continuous case can no longer be used; this gives pseudo-probabilities $\bar{P}(J|I,t)$ of a particle in cell I moving to cell J separated by $\Delta\vec{x}$ as:

$$\bar{P}(J|I,t) = \exp\left(-\frac{\left(\Delta\vec{x}_{IJ} - \vec{v}_I\Delta t\right)^2}{2D\Delta t}\right) \tag{21}$$

To generate probabilities $P(J|I,t)$, the pseudo-probabilities for all cells must be normalized so that the probabilities of movement for *all* particles from any cell *I* sums to unity at each time step and mass is conserved. That is,

$$P(J|I,t) = \frac{\bar{P}(J|I,t)}{\sum_J \bar{P}(J|I,t)} \tag{22}$$

In words, the probability that a particle moves from cell *I* to *J* is equal to the pseudo-probability a particle moves from cell *I* to *J*, divided by the sum of the pseudo-probabilities that that particle moves to any other cell *J*.

The transition matrix that results can then be expressed as a sum of columns:

$$N(J,t+\Delta t) = \sum_{I=1}^{M} \left(\frac{\bar{P}(J|I,t)}{\sum_J \bar{P}(J|I,t)} \right) N(I,t) \tag{23}$$

$$N(J,t+\Delta t) = \sum_{I=1}^{M} [\begin{pmatrix} \frac{\bar{P}(1|I,t)}{\sum_J \bar{P}(J|I,t)} \\ \frac{\bar{P}(2|I,t)}{\sum_J \bar{P}(J|I,t)} \\ \dots \\ \frac{\bar{P}(M|I,t)}{\sum_J \bar{P}(J|I,t)} \end{pmatrix} N(I,t)] \tag{24}$$

Where *M* is the number of cells in the computational domain. This expression can be used to convect each species, even the chemical concentrations, due to the discrete nature of the numerical solution method.

For a non-continuous set of particles, moved through discretized spatial cells in time steps Δt, this expression can be used to express the probability that some number of particles in one cell will move to any other, given the velocity field and initial distribution of particles.

It may appear prohibitive to compute this matrix given that likelihood of movement from one cell to another must be normalized by the likelihood of that movement occurring from the one cell to *every* other; in actuality, the probability of movement to the vast majority of cells will be (for all practical purposes) zero. We can posit a criterion for which probability is immediately set to zero:

$$\frac{\left(\Delta\vec{x}_{IJ} - \vec{v}_{\mathrm{I}}\Delta t\right)^2}{2D\Delta t} \geq \frac{9}{2} \rightarrow \bar{P}(J|I,t) = 0 \rightarrow P(J|I,t) = 0 \tag{25}$$

That is, if the final position of a particle moving from cell *I* to cell *J* is three standard deviations (3σ) or greater from the mean position anticipated, the corresponding pseudo-probability is automatically set to zero. There is a less than 0.3% chance that the particle will end up in all cells that satisfy this criterion, and it is assumed that the probability is so low as to be effectively zero for computational convenience.

Platelet and Chemical Species Implementation

The numerical values and simulation parameters selected to perform the computational analysis of this study will now be described here.

For each of the convected species, the respective diffusion coefficient governs the extent of spread likely observed around the mean location the species tends towards when acted upon by the flowing velocity field of the surrounding blood.

Values for the diffusion coefficients (estimated on the basis of molecular masses M_{r}) were taken from Panteleev et al. [18]; relevant data is shown in Table 3. Platelets were assumed not to diffuse in this study, because they are considerably more massive than all the other species.

Table 3. Diffusion coefficients for convected chemical species (modified from [18]; the diffusion coefficient for IIa-ATIII was added in this study); thrombomodulin (Tm) and its combination with thrombin (IIa-Tm) were not used in this study, but were used in the curve fit

Model variable	M_r	**Diffusion coefficient**	
		(mm^2/min)	**(m^2/s)**
II	72,000	0.0030	$5.0(10^{-11})$
IIa	37,000	0.0040	$6.7(10^{-11})$
AT-III	58,000	0.0033	$5.5(10^{-11})$
IIa-ATIII	95,000	0.0027	$4.5(10^{-11})$
N_a (Platelets)	$\approx 10^{13}$	≈ 0	≈ 0
IIa-Tm	157,000	0.0022	$3.7(10^{-11})$
Tm	120,000	0.0024	$4.0(10^{-11})$

A value for the diffusion coefficient of the aggregate IIa-ATIII was not provided, and was determined using a curve fit to the provided data (see Figure 8).

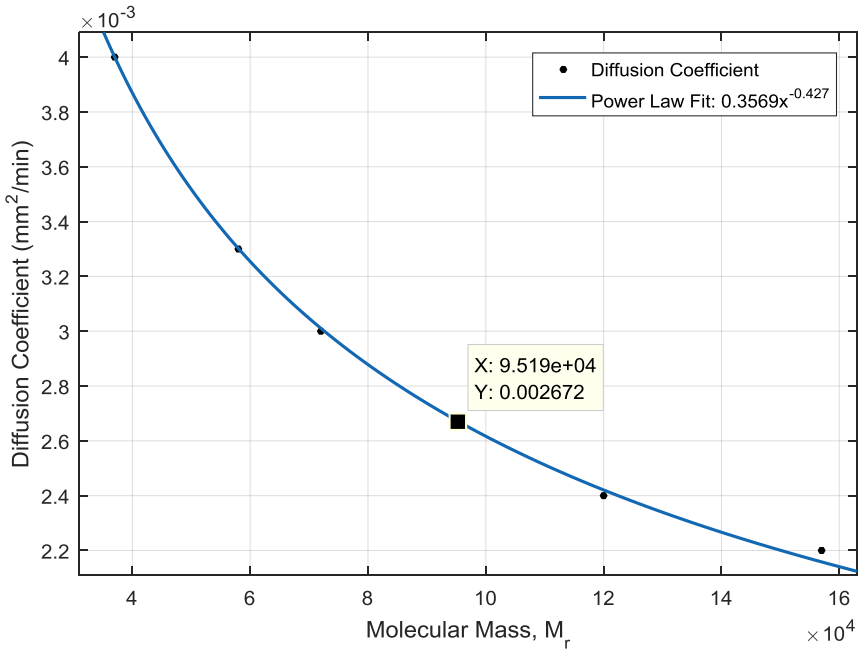

Figure 8. Data and curve fit for molecular mass and its assumed relationship with the diffusion coefficient of relevant species

Spatial Discretization

The combination of diffusion coefficient *D*, time step Δt, and average velocity $\bar{v}$ provide several important guidelines to be considered when selecting simulation parameters such as the spatial discretization for species convection Δx_c (which does not necessarily need to be the same as the spatial discretization for the macroscopic flow simulation, though in this study it is for simplicity).

In particular, Δx_c must be small enough that convected species can actually escape a cell and move to another. The weaker condition requires that they move when acted upon by the velocity field:

$$\Delta x_{advection} \leq v_{max} \Delta t = \left(\frac{5}{4}\right) \bar{v} \Delta t \tag{26}$$

The stronger condition requires that species be able to diffuse out of a cell into another. Considering the diffusion of the particles, if a three-cell spread is desired around the mean, then:

$$\Delta x_{diffusion} \leq \frac{\sqrt{D \Delta t}}{3} \tag{27}$$

Where D is the smallest non-zero diffusion coefficient. Values obtained here (and guidelines in selecting the spatial discretization Δx_c) are (assuming a time step $\Delta t = 0.01$ s):

$$\Delta x_{advection} \approx 4.2 \text{ mm} \tag{28}$$

$$\Delta x_{diffusion} \in [6.38, 8.61](10^{-5}) \text{ mm} \tag{29}$$

It is evident that $\Delta x_{advection}$ and $\Delta x_{diffusion}$ present some conflicting restraints. If Δt is small, then $\Delta x_{diffusion}$ (required to observe any diffusion phenomena) will be prohibitively small. If, on the other hand, Δt is large, then $\Delta x_{advection}$ will be large and convected species will jump the entire length of the domain in a single time step.

Time step $\Delta t = 0.01$ s was selected as an attempt at compromise, and local refinement in the injured area was employed. This allows avoiding ultra-fine simulation everywhere on the one hand or full multi-scale on the other, but this precarious balancing act is clearly a weakness of the transport model that will need to be resolved for more robust implementation in the future.

All cells within the $\Delta x_{advection}$ of the entry of the domain must be initialized each time step with starting concentrations (see Table 1) of all species, because the velocity field would cause entering species to jump over the region otherwise.

Platelet initial concentration is determined assuming 200000 pl/μL or $2.0(10^{14})$pl/m^3, in which case $C_{platelet,initial} = 2.0(10^{14})(\Delta x)^2$. (In a 2D simulation, unit depth is assumed for volume calculations.)

Diffusion Criteria

Diffusion and advection is allowed to occur freely throughout the computational domain, but as cell thrombin levels reach a threshold concentration, local platelets activate, and aggregates form, the flow behavior changes.

In particular, once a cell holds enough activated platelets to be considered a clot, cell viscosity is switched to a high value, slowing local velocity fields to near zero, and trapping platelets (which only move through advection in this model). Chemical species can still diffuse

out of the clotted area, which seems reasonable given the porous nature of the clot. The relevant threshold values are summarized in Table 4.

Table 4. Threshold values used in simulation to determine cell flow and convection behavior. C_{IIa} is the concentration of thrombin in the cell, $N_{platelets}$ is the number of platelets in the cell, μ is the dynamic viscosity

	Criterion:
Add cell to reaction zone	$C_{IIa} > 0$
Activate Cell	$C_{IIa} > 0.1(10^{-6})\text{M}$
Treat cell as clot	$N_{platelets} > \frac{0.40(\Delta\text{x})^2}{V_{platelet}} = \frac{0.40(\Delta\text{x})^2}{\pi(10^{-12})}$
No more platelets allowed in cell	$N_{platelets} > \frac{0.74(\Delta\text{x})^2}{V_{platelet}} = \frac{0.74(\Delta\text{x})^2}{\pi(10^{-12})}$
Clot cell viscosity	$\mu = 10^{30}$
Initialized length	$\Delta x_{advection} = 4.2$ mm

The thrombin cell activation threshold is taken (arbitrarily) as $0.1(10^{-6})\text{M}$; the number of platelets is taken as 40% of the maximum that could be packed into a unit cube with edge length Δx assuming deformation (74% is the ideal packing case for rigid spheres; platelets are deformable, but 74% is taken as the ultimate maximum, to account for porosity).

CHAPTER V

RESULTS

As discussed in the previous section, the time step required to simulate the combined stochastic convection/reduced-order chemical reaction model with a dynamically evolving flow field is small enough to require significant computational cost, simplifications notwithstanding.

In this study, the processes of coagulation are simplified and resolved numerically for a quiescent (zero flow) case, to assess how well the reduced-order model handles the addition of diffusion and inform future work with the model.

The two cases (quiescent and flowing) are contrasted with flow charts detailing the required operations (see Figure 9).

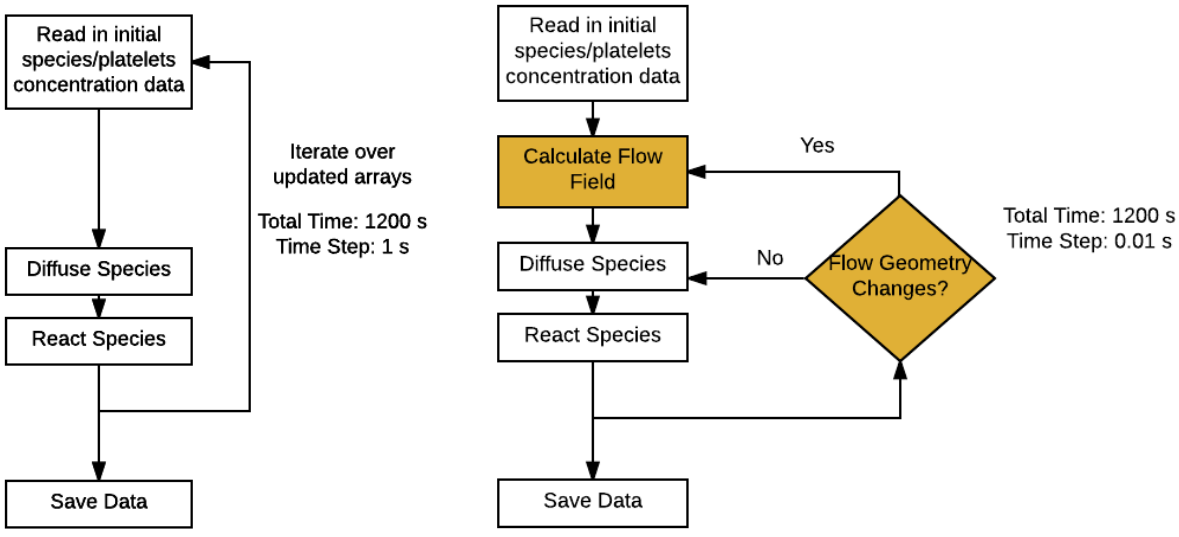

Figure 9. Flow chart showing (a) suggested implementation of the flow model and (b) the actual implementation used for the quiescent model here

It is evident that the two do not differ much in implementation or in terms of the theory required for use; the most important difference is the required time step (and hence the number of evaluations of the transition matrix and reaction model ODEs). The simulation results for the quiescent case are presented below.

Examination of Quiescent Clot Propagation

In the quiescent case, platelet action is neglected due to its (comparatively) small diffusion constant. Thus, cells are considered "activated" (regions in which platelets activate and fibrin precipitates out of the blood) solely dependent on the thrombin concentration.

Reaction is started in a localized "injured" area, and spreads out from there, first increasing and then reducing the concentration of thrombin, consistent with the behavior expected physiologically (Figure 10).

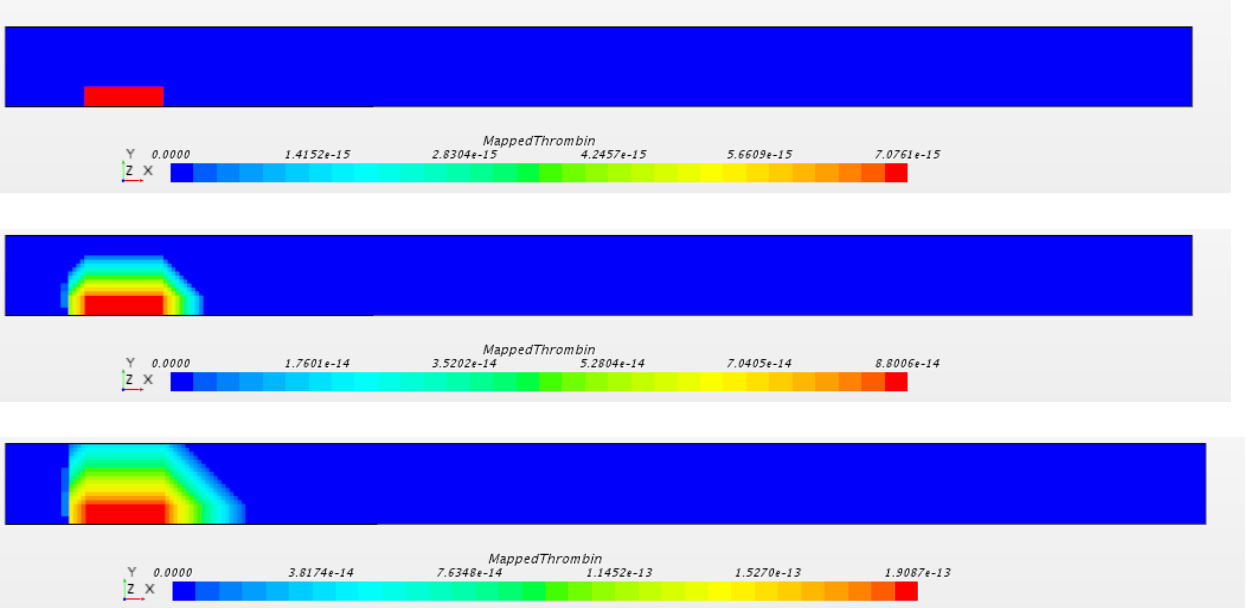

Figure 10. Thrombin increase and diffusion from reaction zone (a) t = 1 s, (b) t = 11s, (c) t = 21s

For the first 530 seconds, thrombin concentration is still too low for anywhere in the region to be considered “activated” (see Figure 4). Shortly after this point, however, thrombin exceeds the critical value and cells begin to be considered likely regions for clots to form, beginning in the injury region and following the diffusing and reacting thrombin outward.

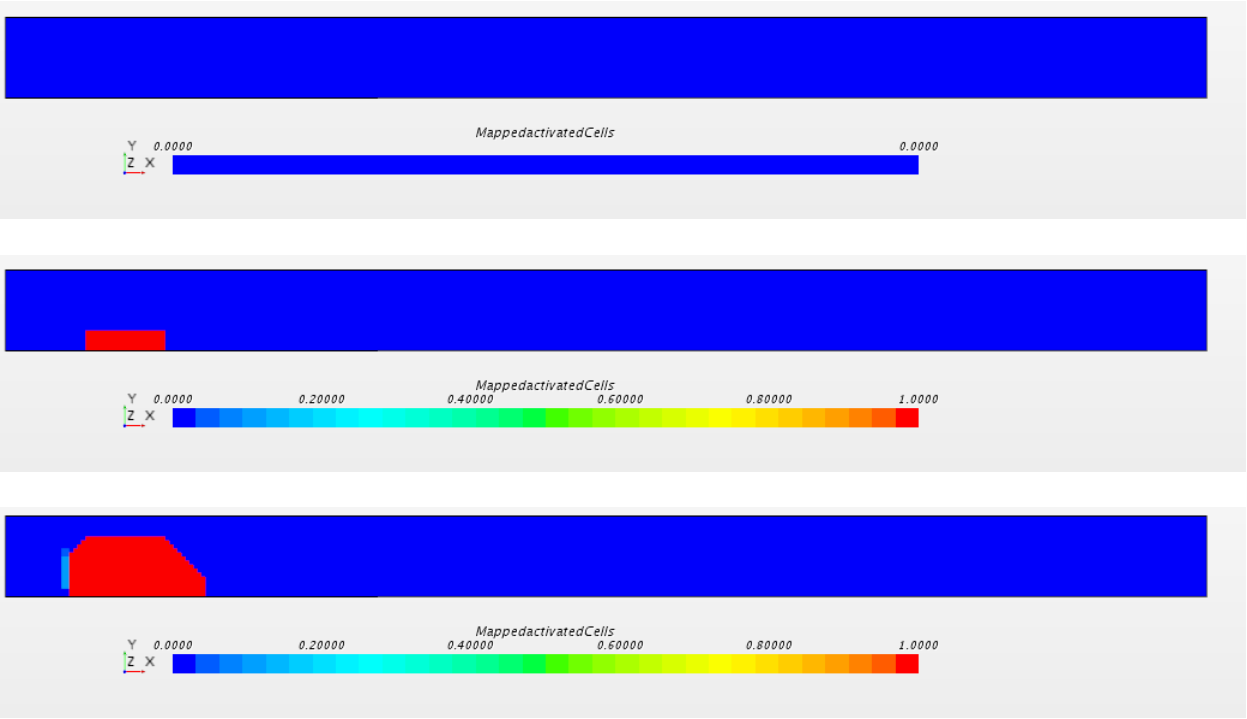

Figure 11. Cell activation at (a) t = 530 s, (b) t = 540 s, (c) t = 550 s

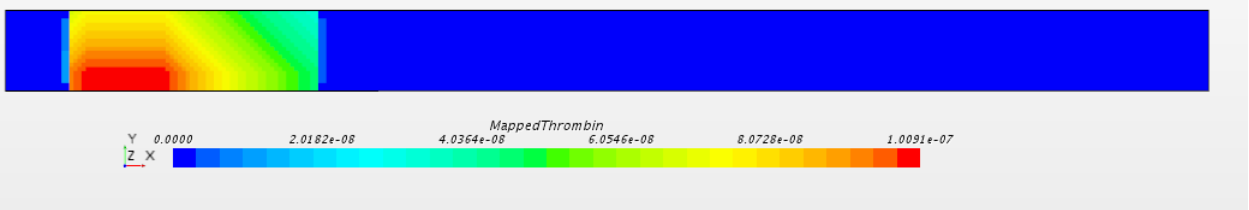

Figure 12. Thrombin concentration at t = 530 s

As the simulation approached 900 s (again, see Figure 4), thrombin, now diffused throughout the entire injury reaction region, begins to decrease in concentration as it is cannibalized by antithrombin (producing IIa-ATIII).

Initially, it was feared that the reduced-order model would diverge to unrealistic large concentration of thrombin with the ability to pull in almost limitless reactants from the surrounding space. In general, however, the reduced-order model exhibited behavior consistent with its 0-dimensional (in space) ordinary differential equation form and, more importantly, physiologically reasonable.

Discussion of Numeric Behavior

As should be clear from the figures above, the reacting species were successfully bound within the ultra-fine reaction region, and did not diffuse through the rest of the domain. This is due to the lengths of the surrounding cells; in the time step provided, it is not probable for the concentrations to jump this discrete length. This limiting behavior can be used to reduce the computational load.

In regards to the computational load, it came disproportionately from use of the transition matrix. (In the domain used, it took ~ 10 times longer for an evaluation of the stochastic diffusion scheme than computation of the reacting species using Euler's method.)

This is somewhat problematic. In a case involving advection, the time step must be made small to compensate for the transition matrix, and ensure physical displacements are made, thus this must be computed at *each* time step. The chemical reactions on the other hand could be computed only every couple of time steps (using a higher-order numerical solver, such as the RK-4 method), but it is unlikely that this would produce significant time savings.

CONCLUSION

In this paper, a framework for less computationally expensive simulation of coagulation phenomena was assembled, and its use was demonstrated for a quiescent (no flow) case. It was shown that the reduced-order reaction model dealt with diffusion well, without catastrophic divergence of thrombin production, but instead with the controlled production and regulation demonstrated by the vascular system.

Work here demonstrated weaknesses of the framework and key areas to focus on to better meet the goal of low computational cost, clinically feasible simulation.

As discussed in previous sections, the spatial discretization required for observation of diffusion and controlled behavior of advection ($\Delta x_{diffusion}$ and $\Delta x_{advection}$) present some conflicting restraints. If Δt is small, then $\Delta x_{diffusion}$ will be prohibitively small. If, on the other hand, Δt is large, then $\Delta x_{advection}$ will be large and convected species will jump the entire length of the domain in a single time step.

This means that selection of time step and spatial discretization require a precarious balancing act, a weakness of the stochastic transport model that will need to be resolved in future, more robust, implementations. Additionally, it was observed that the transition matrix was the most costly operation required, and future work should focus on fine-tuning its performance and evaluating only where necessary.

The combined model has flexibility and reasonable simplification that make it attractive as a basis for patient-specific vascular modeling.

WORKS CITED

[1] K. Perktold and G. Rappitsch, "Computer-Simulation of Local Blood-Flow and Vessel Mechanics in a Compliant Carotid-Artery Bifurcation Model," *J. Biomech.*, vol. 28, no. 7, pp. 845–856, 1995.

[2] C. Tu, M. Deville, L. Dheur, and L. Vanderschuren, "Finite element simulation of pulsatile flow through arterial stenosis," *J. Biomech.*, vol. 25, no. 10, pp. 1141–1152, 1992.

[3] F. J. H. Gijsen, F. N. van de Vosse, and J. D. Janssen, "The influence of the non-Newtonian properties of blood on the flow in large arteries: steady flow in a carotid bifurcation model," *J Biomech*, vol. 32, no. 6, pp. 601–608, 1999.

[4] K. W. Lee and X. Y. Xu, "Modelling of flow and wall behaviour in a mildly stenosed tube," *Med. Eng. Phys.*, vol. 24, no. 9, pp. 575–586, 2002.

[5] K. Perktold, M. Resch, and R. O. Peter, "Three-dimensional numerical analysis of pulsatile flow and wall shear stress in the carotid artery bifurcation," *J. Biomech.*, vol. 24, no. 6, pp. 409–420, 1991.

[6] S. Z. Zhao, X. Y. Xu, and M. W. Collins, "The numerical analysis of fluid-solid interactions for blood flow in arterial structures. Part 2: Development of coupled fluid-solid algorithms.," *Proc. Inst. Mech. Eng. H.*, vol. 212, no. 4, pp. 241–252, 1998.

[7] S. Z. Zhao, X. Y. Xu, A. D. Hughes, S. A. Thom, A. V. Stanton, B. Ariff, and Q. Long, "Blood flow and vessel mechanics in a physiologically realistic model of a human carotid arterial bifurcation," *J. Biomech.*, vol. 33, no. 8, pp. 975–984, 2000.

[8] K. G. Mann, S. Butenas, and K. Brummel, "The dynamics of thrombin formation," *Arterioscler. Thromb. Vasc. Biol.*, vol. 23, no. 1, pp. 17–25, 2003.

[9] C. M. Danforth, T. Orfeo, S. J. Everse, K. G. Mann, and K. E. Brummel-Ziedins, "Defining the boundaries of normal thrombin generation: Investigations into hemostasis," *PLoS One*, vol. 7, no. 2, 2012.

[10] A. L. Fogelson, "A mathematical model and numerical method for studying platelet adhesion and aggregation during blood clotting," *J. Comput. Phys.*, vol. 56, no. 1, pp. 111–134, 1984.

[11] Z. Xu, N. Chen, M. M. Kamocka, E. D. Rosen, and M. Alber, “A multiscale model of thrombus development.,” *J. R. Soc. Interface*, vol. 5, no. 24, pp. 705–22, 2008.

[12] M. H. Flamm, T. V Colace, M. S. Chatterjee, H. Jing, S. Zhou, D. Jaeger, L. F. Brass, T. Sinno, and S. L. Diamond, “Multiscale prediction of patient-specific platelet function under flow,” vol. 120, no. 1, pp. 190–199, 2017.

[13] M. Anand, K. Rajagopal, and K. R. Rajagopal, “A Model Incorporating Some of the Mechanical and Biochemical Factors Underlying Clot Formation and Dissolution in Flowing Blood,” *J. Theor. Med.*, vol. 5, no. 3–4, pp. 183–218, 2003.

[14] “Star-CCM+.” Siemens, Melville, NY, 2017.

[15] S. Z. Zhao, B. Ariff, Q. Long, A. D. Hughes, S. A. Thom, A. V. Stanton, and X. Y. Xu, “Inter-individual variations in wall shear stress and mechanical stress distributions at the carotid artery bifurcation of healthy humans,” *J. Biomech.*, vol. 35, no. 10, pp. 1367–1377, 2002.

[16] Joe D., “Coagulation with arrows for negative and positive feedback,” *Wikipedia*. [Online]. Available: https://commons.wikimedia.org/w/index.php?curid=1983833%0A. [Accessed: 11-Oct-2016].

[17] J. Arumugam, “Reduced-Order Coagulation Model,” 2017.

[18] M. A. Panteleev, M. V. Ovanesov, D. A. Kireev, A. M. Shibeko, E. I. Sinauridze, N. M. Ananyeva, A. A. Butylin, E. L. Saenko, and F. I. Ataullakhanov, “Spatial Propagation and Localization of Blood Coagulation Are Regulated by Intrinsic and Protein C Pathways, Respectively,” *Biophys. J.*, vol. 90, no. 5, pp. 1489–1500, 2006.